NANO LETTERS

2008
Vol. 8, No. 5
1386-1392

Controlled Growth of Ternary Alloy Nanowires Using Metalorganic Chemical Vapor Deposition

Sung K. Lim, Michael J. Tambe, Megan M. Brewster, and Silvija Gradečak*

Department of Materials Science and Engineering, Massachusetts Institute of Technology, Cambridge, Massachusetts 02139

Received January 14, 2008; Revised Manuscript Received February 28, 2008

ABSTRACT

We report the growth and characterization of ternary $Al_xGa_{1-x}As$ nanowires by metalorganic chemical vapor deposition as a function of temperature and V/III ratio. Transmission electron microscopy and energy dispersive X-ray spectroscopy show that, at high temperatures and high V/III ratios, the nanowires form a core–shell structure with higher Al composition in the nanowire core than in the shell. We develop a growth model that takes into account diffusion of reactants and decomposition rates at the nanowire catalyst and stem to describe the compositional difference and the shell growth rate. Utilizing this model, we have successfully grown compositionally uniform $Al_{0.16}Ga_{0.84}As$ nanowires. The ability to rationally tune the composition of ternary alloy nanowires broadens the application range of nanowires by enabling more complex nanowire heterostructures.

Nanowires are quasi-one-dimensional single crystals with lateral dimensions that can be scaled down to only a few nanometers while maintaining micrometer lengths. Semiconductor nanowires can simultaneously act as active components and interconnects and therefore have emerged as versatile building blocks for applications in nanoscale electronics, photonics, and biosensing.[1] For these applications, growth of single-composition elemental and binary semiconductor nanowires has been demonstrated for a variety of materials including Si and Ge,[2] GaN,[3] GaAs,[4] GaP,[5] and InAs.[6] Ternary alloy nanowires offer an advantage over single-composition or binary nanowires in terms of the ability to tune the energy band gap by adjusting the relative composition of the alloy. The controlled synthesis of ternary alloy nanowires would therefore broaden the application range of nanowires by enabling more complex architectures including axial[7] and radial heterostructures.[8,9] In particular, development of $Al_xGa_{1-x}As$ nanowires has significant importance in nanowire photonics and electronics. The ability to tune the emission wavelength in the range from infrared to red would be important in applications involving nanowire light emitting diodes,[10] lasers,[3] single photon sources,[11] or wavelength shifters,[12] while the intrinsically higher band gap of AlGaAs than GaAs or InGaAs would be valuable for development of nanowire-based high electron mobility transistors.[13]

Despite the obvious advantages of ternary nanowires in comparison to the elemental and binary semiconductor nanowires, their controlled growth is far from being elucidated due to the complex thermodynamic and kinetic phenomena that compete during the growth process.[14] The vapor–liquid–solid (VLS) mechanism is the commonly accepted mechanism of the single crystalline nanowire growth.[2,15] During the anneal above the eutectic point, the nanosized catalysts such as gold form liquid droplets that alloy with reactant materials supplied from the gas phase or by diffusion from the growth substrate and nanowire sidewalls. Subsequently, the liquid droplets reach the point of supersaturation and the reagent material is anisotropically solidified in the direction of low kinetic energy (e.g., ⟨111⟩ direction). Although the catalytic effect accounts for faster nucleation and chemical reactions, improved decomposition of materials, and greater adsorption rate,[16] the dominant growth mechanism depends on the growth technique, materials, and growth conditions. For example, the growth of GaP nanowires by metalorganic chemical vapor deposition (MOCVD) varies from a diffusion limited process to synergetic effect limiting process that depends on the spacing between the nanowires,[17] while growth of Si nanowires by gas phase epitaxy is dominated by direct impingement of atoms at the catalyst tip.[18] In contrast, GaAs nanowire growth by molecular beam epitaxy (MBE) and MOCVD is controlled by the diffusion of reactant sources.[19,20]

In this paper, we study the growth mechanism of $Al_xGa_{1-x}As$ nanowires grown by MOCVD in terms of compositional gradient along the nanowire lengths and based on the diffusion-induced model of GaAs nanowires.[20] We observe that these nanowires exhibit tapering morphology and a compositional gradient along their length. We then show that both the tapering and the gradient are caused by

* Corresponding author. E-mail: gradecak@mit.edu.

10.1021/nl080129n CCC: $40.75
Published on Web 04/04/2008

a spontaneous core–shell structure of two different but uniform compositions of $Al_xGa_{1-x}As$. Finally, we study the effects of varying growth temperature and V/III ratio on the competing growth mechanisms for realization of $Al_xGa_{1-x}As$ nanowires with uniform composition.

$Al_xGa_{1-x}As$ nanowires were grown by cold-walled horizontal-flow atmospheric pressure MOCVD and the approach was based on the growth of single-crystal, uniform, and defect-free GaAs nanowires grown on (100)B GaAs substrate at 420–480 °C.[21] For Au-assisted growth, 1 nm Au film was evaporated on (100)B and (111)B GaAs growth substrates. After loading the sample into the reactor chamber, the sample was heated up to 600 °C and annealed for 10 min in hydrogen (H_2) and arsine (AsH_3) flow to remove the oxide layer. The nanowire growth was initiated by reducing the temperature to 380–480 °C and then simultaneously introducing trimethylgallium (TMG) and trimethylaluminum (TMA). During the growth, H_2 carrier gas flow was kept constant at 15 slm (standard liters per minute), TMG and TMA flows were 18.8 and 3.1 μmol/min, respectively, while AsH_3 flow was varied in the range of 120−2200 μmol/min to tune the V/III ratio from 5.5 to 100. Unless otherwise indicated, all nanowires were grown for 20 min.

The morphology of as-grown samples was studied using a JEOL 6320FV high-resolution scanning electron microscope (SEM) in secondary electron mode. High-resolution lattice image and the composition of nanowires were characterized by a JEOL 2010F field-emission transmission electron microscope (FE-TEM) equipped with energy dispersive X-ray spectroscopy (EDS). For scanning transmission electron microscopy (STEM) bright-field and annular dark-field imaging, as well as EDS line-scan analysis, a VG HB603 FE STEM was used operating at 250 kV.

Figure 1a shows SEM images of $Al_xGa_{1-x}As$ nanowires grown on GaAs (100)B substrates at 480 °C with V/III ratio of 80. The nanowires are 1–2 μm long with distribution of diameters in the range of 20−70 nm (measured directly below the catalytic particle) and have highly tapered morphology with the diameter gradually increasing from the catalyst to the base of the nanowire. High-resolution TEM images and selected area diffraction patterns reveal a single-crystal zincblende structure of the nanowires grown along the ⟨111⟩ direction, while lower resolution bright-field TEM and dark-field STEM images indicate a defect-free structure (Figure 1b). Interestingly, EDS spectra taken at different nanowire regions show significant compositional gradient along the nanowire length with increasing atomic Al percentage (x in $Al_xGa_{1-x}As$ ternary system) in the direction of the nanowire growth (Figure 1c).

To further elucidate the origin of the compositional change, we recorded EDS line-scan profiles across the nanowire diameter at different axial positions of the nanowire (Figure 2). These results show distinct spatial profiles for Ga and Al and indicate spontaneous formation of a core–shell nanowire structure where the Al percentage is higher in the core than in the shell. To fit the EDS line profiles, we developed a nanowire core–shell model based on top-view SEM images (Figure 3a) consisting of an equilateral hexagonal core and a nonequilateral hexagonal shell[22] with distinct and constant aluminum compositions and negligible diffusion across the core–shell interface (Figure 3b). The model is in excellent agreement with the experimentally measured profiles (Figures 2b−d), with the best fit obtained for a nanowire with a core diameter of 22 nm, Al composition in the core $x_{core} = 0.30$, aluminum composition in the shell $x_{shell} = 0.10$, and gradually increasing shell thickness from 0 to 85 nm at the nanowire top and bottom, respectively.

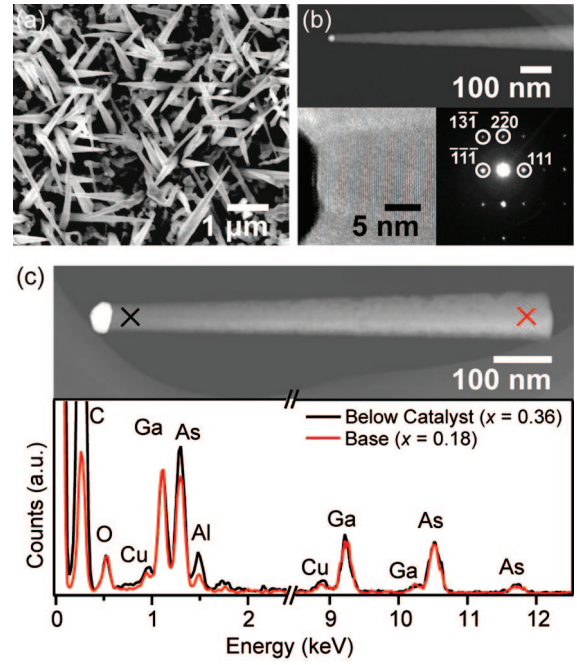

Figure 1. Structure of $Al_xGa_{1-x}As$ nanowires grown on (100) GaAs substrates at 480 °C and with V/III ratio of 80. (a) Plan view SEM image shows 1–2 μm long nanowires with tapered morphology. (b) STEM image (top), high-resolution TEM image (bottom left) and corresponding selected-area diffraction pattern (bottom-right) along ⟨11−2⟩ zone axis indicating defect-free zincblende structure and ⟨111⟩ growth direction. (c) STEM image and EDS spectra collected at two points along the nanowire axis (indicated by markers). The EDS spectra were normalized to Ga-L line at 1.1 keV. The nanowires exhibit compositional gradient along the nanowire length with higher Al composition at the nanowire top ($x = 0.36$) than at the base ($x = 0.18$).

The EDS results show that the core and shell have constant but distinct compositions; together with the tapering morphology, this fact suggests that the gradient of the total Al composition along the nanowire growth direction is due to the gradual change of the shell thickness. To further confirm this hypothesis, we used the nanowire model represented in Figure 3b and eq 1 to calculate $x_{overall}$, the overall Al composition at the axial position L (Figure 3b):

$$x_{overall} = \frac{x_{shell}(D_{out}^2 g_{ne} - D_{in}^2 g_e) + x_{core}(D_{in}^2 g_e)}{D_{out}^2 g_{ne}} \cong \frac{x_{shell}(D_{out}^2 - D_{in}^2) + x_{core} D_{in}^2}{D_{out}^2} \quad (1)$$

where D_{out} and D_{in} are defined as the cross-sectional diameters of the nanowire and its core at the position L, respectively. The ratio of geometrical factors of nonequilateral hexagon (g_{ne}) and that of equilateral hexagon (g_e) is

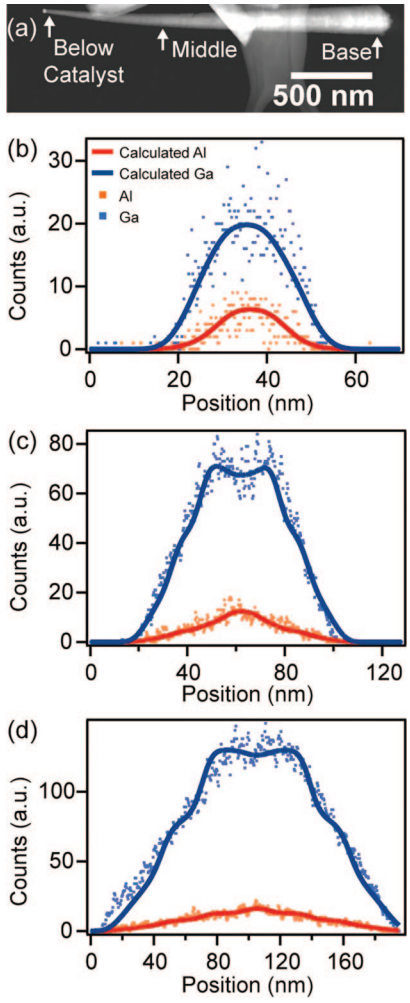

Figure 2. EDS line profiles of $Al_xGa_{1-x}As$ nanowire grown at 480 °C and with V/III ratio of 80. (a) STEM image with arrows indicating cross-section sites of EDS line-scans. (b−d) Corresponding EDS cross-section line profiles for Al (red symbols) and Ga (blue symbols) recorded (b) below the catalyst, (c) in the middle, and (d) at the base of the nanowire. The experimental results were fitted (solid lines) to a core–shell nanowire model consisting of equilateral hexagon-shaped core and nonequilateral hexagon-shaped shell assuming a Gaussian electron probe profile of 3 nm fwhm and no absorption effects.

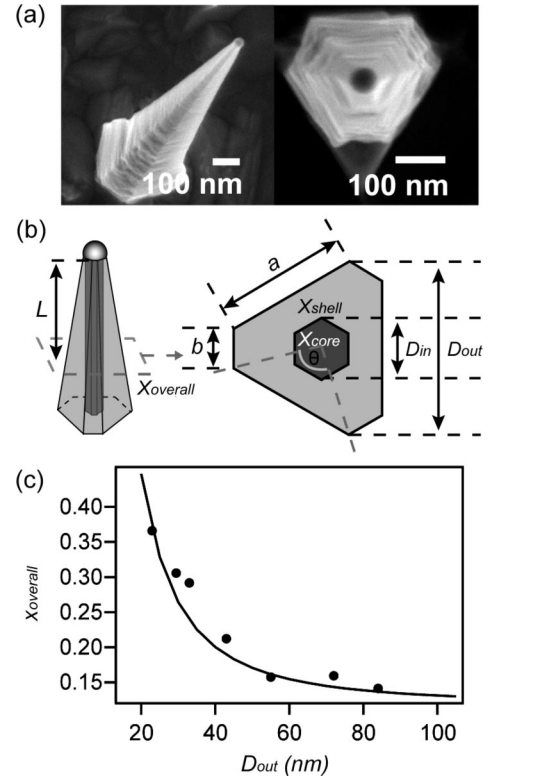

Figure 3. (a) Side and plan view SEM images of a single $Al_xGa_{1-x}As$ nanowire nanowire grown at 480 °C and with V/III ratio of 80. (b) Schematic model of $Al_xGa_{1-x}As$ nanowire core–shell structure based on SEM images shown in (a). Nonequilateral hexagon shell consists of three longer sides with length a and three shorter sides with length b. The overall diameter is D_{out} and the measured angle $\theta \approx 78°$. The core has equilateral hexagon shape with diameter D_{in}. (c) Measured $x_{overall}$ as a function of D_{out} (symbols) and the model fit using eq 1 (solid line).

$0.975 \approx 1$ for $\theta \approx 78°$ (see Figure 3b), and thus $x_{overall}$ can be approximately described in terms of x_{shell}, x_{core}, D_{out}, and D_{in}. The $x_{overall}$ was quantified from EDS line-scans at position L, while the x_{core} was measured from EDS data just below the catalyst, and these results were used to calculate x_{shell}. Figure 3c shows the result of this analysis and represents $x_{overall}$ as a function of total nanowire width at various points along the nanowire length. The best fit to the experimentally measured results corresponds to $x_{shell} = 0.11$, which is in excellent agreement with our EDS linescan simulations presented in Figure 2.

A similar tapering phenomenon has been observed in binary GaAs nanowires[23] and was attributed to the presence of two competing growth mechanisms: the catalyzed VLS mechanism responsible for axial elongation of nanowires and the vapor−solid (VS) mechanism in which the precursors decompose and incorporate directly into the nanowire sidewalls. The fact that the VLS core and the VS shell have different but uniform compositions for our AlGaAs ternary alloy nanowires indicates that the relative Al and Ga incorporation rates are different for these two growth mechanisms. Figure 4 schematically illustrates VLS and VS growth mechanisms in the case of MOCVD, where growth rates of both processes depend on the decomposition of metalorganic (MO) precursors at the catalyst and nanowire stem as well as adatom diffusion.

To determine the relative contributions of the adatom diffusion and MO source decomposition for the VS and VLS processes, we studied the influence of the temperature and V/III ratio on the tapering and compositional change of the nanowires. The total thickness of the shell at the nanowire base $(D_{out} - D_{in})_{base}$ was used as a measure of the amount of the shell deposition. It should be noted that the thickness of the shell at the nanowire base depends on the total nanowire length (L_{Nw}). On the basis of the linear dependence of $D_{out} - D_{in}$ and L (inset of Figure 5a), we introduce the tapering factor (eq 2) as a figure of merit that describes the effect of altering process parameters on the degree of the VS deposition:

$$TF = \frac{(D_{out} - D_{in})_{base}}{L_{Nw}} \quad (2)$$

To investigate the effect of temperature on the composition, III/V ratio was kept constant (80) and the growth

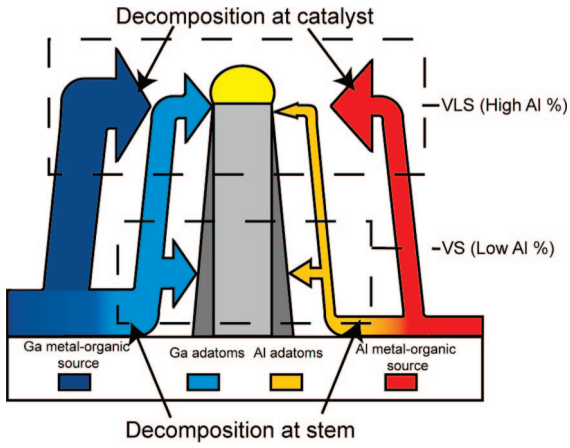

Figure 4. Schematic illustration of the $Al_xGa_{1-x}As$ nanowire growth using MOCVD. The nanowire shell growth rate by VS mechanism is proportional to the amount of adatoms created by decomposition of MO precursors (TMG and TMA) at nanowire stem and inversely proportional to the diffusion length of the adatoms. At the stem, Al adatoms have shorter diffusion lengths but lower decomposition rate than Ga adatoms, resulting in the low x_{shell}. VLS growth mechanism is responsible for x_{core} and depends on the adatom diffusion and MO precursor decomposition at the catalyst. Adatom contribution tends to lower x_{core} relative to x_{shell} due to short diffusion length of Al adatoms. However, relatively high concentration of TMA and higher decomposition rate at the catalyst results in higher x_{core} than x_{shell}.

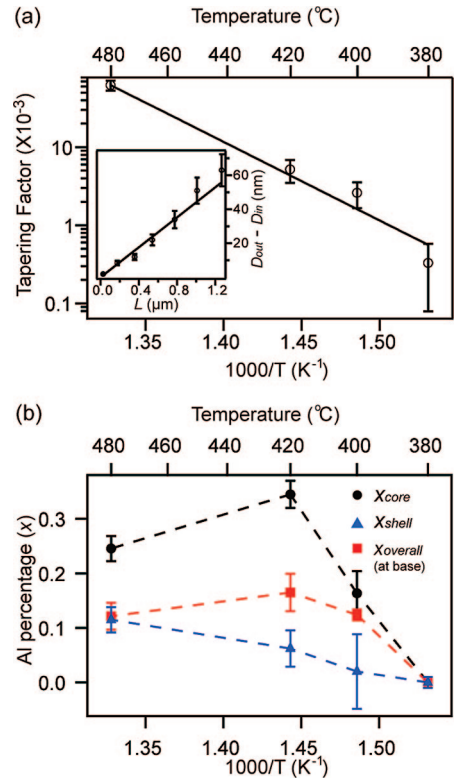

Figure 5. (a) Temperature dependence of the tapering factor, as defined in eq 2. During the growth, the V/III ratio was kept at 80. Symbols represent experimental measurements, while the solid line corresponds to an exponential fit. Inset: measured shell thickness along the nanowire length (symbols) and the linear fit (solid line). (b) Temperature dependence of x_{core}, x_{shell}, and $x_{overall}$. The experimental x_{core} and $x_{overall}$ (symbols) were obtained from EDS spectra with spot size of 100 nm below the catalyst and at base of nanowires, respectively, while x_{shell} was calculated using eq 1. Dashed lines are guides to the eye.

temperature varied in the range of 380−480 °C. Figure 5a shows that the tapering factor increases exponentially as the growth temperature is increased, indicating that shell growth is a thermal activated process with the calculated activation energy of 46 kcal/mol. Simultaneously, x_{shell} increased almost linearly with temperature over the entire measured temperature range (Figure 5b).

Both the tapering factor and composition gradient increase with increasing temperature, which supports the following model of the nanowire shell growth (more detailed description of the model is provided in the Supporting Information). Because of the short diffusion lengths of decomposed Ga and Al adatoms,[24,25] these species will likely be incorporated onto the nanowire sidewalls via VS before reaching the catalyst. The incorporation of Al and Ga at the sidewalls by VS is proportional to the amount of adatoms decomposed at the stem, which is the product of the concentration of gas sources and the decomposition rate at the stem and inversely proportional to the diffusion length of adatoms (eq S1, Supporting Information). Al adatoms have shorter diffusion length than Ga adatoms, but the decomposition rate of TMA into adatoms is much slower than that of TMG because of the high bond strength of $Al-CH_3$ (65 kcal/mol) compared to $Ga-CH_3$ (57 kcal/mol).[26] Consequently, the shell has low Al composition, as shown in Figure 5b. Precursor decomposition is a thermally activated process and increasing temperature enhances the decomposition at the nanowire stem, which results in an increased amount of adatoms and a consequent enhancement of the VS deposition. Simultaneously, the relative ratio of decomposed TMA and TMG at the nanowire stem increases with temperature due to higher bonding energy of TMA (Figure S1, Supporting Information), thus increasing the aluminum composition in the shell, similarly to the case of composition variation of $Al_xGa_{1-x}As$ thin film.[27]

In contrast to the VS growth described above, the VLS growth of the nanowire core shows a different tendency. Al composition in the nanowire core increases linearly up to 420 °C and then starts to decrease with further increase of temperature (Figure 5b). In the case when adatom diffusion is the dominant factor of the VLS growth, as observed in gas source MBE-grown AlGaAs nanowires,[24] x_{core} is lower than x_{shell} due to shorter diffusion length of Al adatoms relatively to Ga. However, to account for the opposite tendency observed in our nanowires, we suggest that the decomposition and incorporation of the MO precursors at the catalyst is the dominant VLS process for the MOCVD growth. The catalyst particle acts as an efficient decomposition site because a liquid catalyst decomposes the trimethyl precursors to monomethyl precursors,[17] which are more likely to decompose into adatoms. The incorporation into the nanowire core is then proportional to the amount of undecomposed MO precursors that reach the catalyst and their decomposition rate (eq S3, Supporting Information). The amount of precursors that reach and decompose at the catalyst is strongly linked to the amount of undecomposed MO

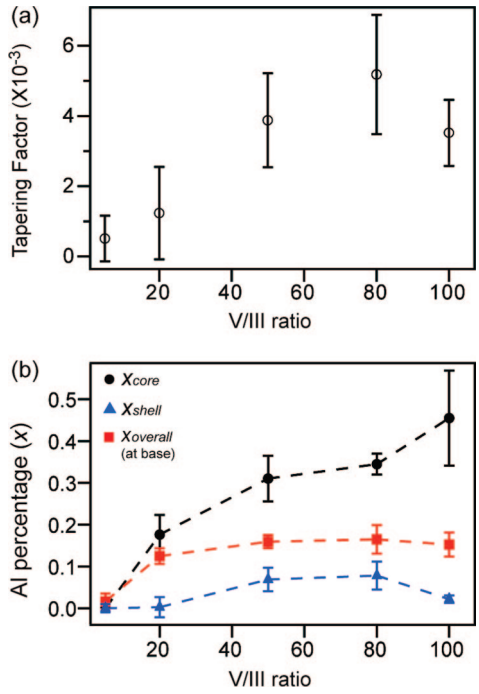

Figure 6. V/III dependence of (a) the tapering factor and (b) x_{core}, x_{shell}, and $x_{overall}$. During the growth, the temperature was kept at 420 °C. The x_{core} and $x_{overall}$ were obtained from EDS spectra with spot size of 100 nm below the catalyst and at base of nanowires, respectively, while x_{shell} was calculated using eq 1. Dashed lines are guides to the eye.

precursors at the nanowire stem. As described above, at low temperature range (380−420 °C), decomposition of MO precursors at the nanowire stem is low and these are more likely to reach the catalyst. As the temperature increases, the ratio of the arriving undecomposed TMA to TMG amount decreases, but the ratio of TMA and TMG decomposition rate at the catalyst simultaneously increases. From the small tapering factor (i.e., low decomposition at the sidewalls) in the low temperature range, we conclude that the effect of the decomposition term is more dominant than the MO arriving term, resulting in the overall increase of x_{core} with temperature. However, at temperatures above 420 °C, the decomposition at the nanowire stem generates a significant amount of adatoms, resulting in a maximum and subsequent lowering of x_{core}. This temperature tendency of the x_{core} variation is consistent with the temperature-dependent growth rate in GaAs binary system, where the growth is decomposition dominant at low temperatures, and diffusion influenced at high temperatures.[23] Taken together, the degree of the compositional gradient for nanowires grown at low temperatures is small because of the small tapering and $x_{overall}$ can be approximated by x_{core}. In contrast, significantly tapered nanowires grown at high temperatures have a large compositional gradient.

To investigate the effect of V/III ratio on the composition, we maintained a constant temperature of 420 °C and varied V/III ratio in the range of 5−100 by increasing AsH_3 flow at fixed group III flow. Figure 6a shows that the tapering factor increases up to V/III of 80, where it exhibits a maximum and then decreases. This result can be explained using similar arguments as discussed above (eq S6, Supporting Information). Increasing the V/III ratio decreases the diffusion length of TMG and TMA up to a V/III ratio of 80 by reducing the lifetime of species[28] and enhances the decomposition of TMG and TMA.[29] In the presence of AsH_3, TMG and TMA form $(CH_3)_{3-x}GaAsH_{3-y}$ and $(CH_3)_{3-x}AlAsH_{3-y}$ complexes, which subsequently decompose to GaAs and AlAs on the surface.[29] Consequentially, as the V/III ratio is increased, the total incorporation of Ga and Al at the nanowire sidewalls increases up to a critical point (As-assisted decomposition). For even higher AsH_3 flows, As stabilizes the nanowire surface and prevents the incorporation of Ga and Al adatoms into the crystal (As-stabilized effect).[30] The As-assisted decomposition and decreasing lifetime compete against the As-stabilized effect, resulting in a maximum of the incorporation rate at the nanowire stem at V/III = 80. For further increase of the V/III ratio, the As-stabilized growth becomes significant, reducing the overall shell deposition (Figure S3, Supporting Information).

Figure 6b shows the influence of V/III ratio on x_{shell} exhibiting a similar tendency to the tapering factor. In the As-assisted decomposition regime, the higher bonding energy of TMA compared to TMG makes the decomposition of TMA more sensitive to V/III ratio, resulting in an increase of x_{shell} due to As-assisted effects for relatively low V/III ratio. The As-stabilized effect is stronger for Al-species than for Ga-species because the cohesive energy of Al−As (8.5469 eV) is larger than that of Ga−As (7.6987 eV)[31] and for high V/III ratio x_{shell} decreases by competition of As-assisted and As-stabilized surface effects. On the other hand, x_{core} shows a different tendency and increases continuously with V/III ratio (Figure 6b) because the VLS process does not involve the surface incorporation term. This means that VLS is only dependent on the As-assisted decomposition term, which is also consistent with the higher growth rate observed for high V/III ratio in binary GaAs nanowires.[4] As a result, x_{core} increases continuously with AsH_3 flow. From these results we conclude the tapering effect and the difference between x_{shell} and $x_{overall}$ are minimized for low V/III ratios, which in turn improves the overall compositional homogeneity of the nanowires.

Spontaneously formed core–shell nanowires could be used for applications in electronics[13] and photonics.[9] However, only the controlled growth of ternary alloy nanowires will realize the full potential of radial and axial nanowire heterostructures. We therefore utilized the knowledge of the growth kinetics gained through temperature and V/III ratio measurements to demonstrate growth of AlGaAs nanowires with uniform composition. Parts a and b of Figure 7 show straight $Al_{0.16}Ga_{0.84}As$ nanowires grown at low temperature (420 °C) and low and V/III ratio (20) in order to minimize the compositional gradient along the nanowire length. The average compositional difference from the catalyst to the base is 0.02 for nanowires grown for 20 min ($L_{Nw} \sim 4$ μm) and only 0.01 for nanowires grown for 5 min ($L_{Nw} \sim 1$ μm), as shown in Figure 7a−c. In this regime, the tapering is minimized while the core composition is mainly governed

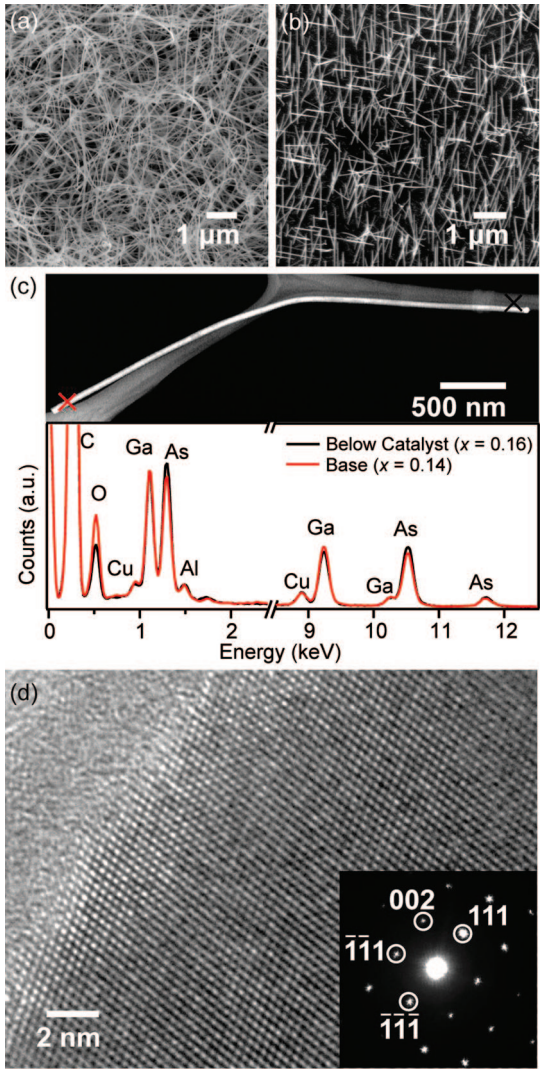

Figure 7. SEM images of compositionally uniform $Al_{0.16}Ga_{0.84}As$ nanowires grown on (100) GaAs substrates at 420 °C with V/III ratio of 20 for (a) 20 min and (b) 5 min. (c) STEM image and corresponding EDS spectra. Markers on the image indicate spectra accumulation sites. The EDS spectra were normalized to Ga-L line at 1.1 keV. (d) High-resolution TEM image and corresponding selected-area diffraction pattern (inset) along the ⟨1−10⟩ zone axis indicate the nanowires grow along the ⟨111⟩ direction and have zincblende structure.

by TMG and TMA diffusion along the nanowire sidewalls and decomposition at the catalyst. Therefore the x_{core} is proved constant along the nanowire, which is consistent with our model. These compositionally uniform nanowires have single crystal zincblende structure, do not contain any structural defects and grow along ⟨111⟩ direction (Figure 7d).

In conclusion, by elucidating the competing growth processes involved in the MOCVD growth of ternary compound nanowires, we were able to grow $Al_xGa_{1-x}As$ by MOCVD with negligible tapering, no atomic stacking faults, and uniform composition. The complex growth processes at the catalyst particles and nanowire stem can lead to the spontaneous formation of tapered core–shell structures and subsequent compositional nonuniformity along the nanowire length. Incorporation of Al and Ga at the nanowire sidewalls (VS) is governed by decomposition of metalorganic sources and resultant adatom diffusion, while incorporation at the catalyst (VLS) is determined by the amount of MO precursors, Ga and Al adatoms, and the catalytically enhanced decomposition rate. All of these processes are functions of the growth conditions including V/III ratio and temperature, so we developed a growth model that allowed us the control over nanowire growth. Tapering and compositional inhomogeneities were minimized by utilizing low V/III ratio, and low temperature and successful growth of uniform $Al_{0.16}Ga_{0.84}As$ nanowires was demonstrated. Further research is under way that will take advantage of relative TMA and TMG flows for the growth of uniform and compositionally tunable $Al_xGa_{1-x}As$ nanowires.

Acknowledgment. We thank Professor E. Fitzgerald for the access to the MOCVD facilities and the MIT Center for Materials Science and Engineering, NSF-funded MRSEC, for the use of electron microscopy facilities. S.K.L. and M.B. acknowledge the Cambridge Foundation and the National Science Foundation, respectively, for the Graduate Research Fellowship support. S.G. acknowledges MIT startup funds.

Supporting Information Available: A model for the growth of ternary alloy nanowires using MOCVD. This material is available free of charge via the Internet at http://pubs.acs.org.

References

(1) (a) Lieber, C. M. *MRS Bull.* **2003**, *28*, 486. (b) Thelander, C.; Agarwal, P.; Brongersma, S.; Eymery, J.; Feiner, L. F.; Forchel, A.; Scheffler, M.; Riess, W.; Ohlsson, B. J.; Gösele, U.; Samuelson, L. *Mater. Today* **2006**, *9*, 28. (c) Yang, P *MRS Bull.* **2005**, *30*, 85. (d) Lieber, C. M.; Wang, Z. L. *MRS Bull.* **2007**, *32*, 99. (e) Patolski, F.; Timko, B. P.; Zheng, G.; Lieber, C. M. *MRS Bull.* **2007**, *32*, 142.
(2) Morales, A. M.; Lieber, C. M. *Science* **1998**, *279*, 208.
(3) Gradečak, S.; Qian, F.; Li, Y.; Park, H. G.; Lieber, C. M. *Appl. Phys. Lett.* **2005**, *87*, 173111.
(4) Borgström, M. T.; Deppert, K.; Samuelson, L.; Seifert, W. *J. Cryst. Growth* **2004**, *260*, 18.
(5) Dick, K. A.; Deppert, K.; Martensson, T.; Seifert, W.; Samuelson, L. *J. Cryst. Growth* **2004**, *272*, 131.
(6) Dayeh, S. A.; Yu, E. T.; Wang, D. *Nano Lett.* **2007**, *7*, 2486.
(7) (a) Gudiksen, M. S.; Lauhon, L. J.; Wang, J.; Smith, D. C.; Lieber, C. M. *Nature* **2002**, *415*, 617. (b) Björk, M. T.; Ohlsonn, B. J.; Sass, T.; Personn, A. I.; Thelander, C.; Magnusson, M. H.; Deppert, K.; Wallenberg, L. R.; Samuelson, L. *Nano Lett.* **2002**, *2*, 87. (c) Wu, Y.; Fan, R.; Yang, P. *Nano Lett.* **2002**, *2*, 83.
(8) Lauhon, L. J.; Gudiksen, M. S.; Wang, C. L.; Lieber, C. M. *Nature* **2002**, *420*, 57.
(9) Qian, F.; Li, Y.; Gradečak, S.; Wang, D. L.; Barrelet, C. J.; Lieber, C. M *Nano Lett.* **2004**, *4*, 1975.
(10) Qian, F.; Gradečak, S.; Li, Y.; Wen, C. Y.; Lieber, C. M. *Nano Lett.* **2005**, *5*, 2287.
(11) Borgström, M. T.; Zwiller, V.; Müller, E.; Imamoglu, A. *Nano Lett.* **2005**, *5*, 1439.
(12) Fluegel, B.; Mascarenhas, A.; Snoke, D. W.; Pfeiffer, L. N.; West, K. *Nat. Photon.* **2007**, *1*, 701.
(13) Li, Y.; Xiang, J.; Qian, F.; Gradečak, S.; Wu, Y.; Yan, H.; Blom, D. A.; Lieber, C. M. *Nano Lett.* **2006**, *6*, 1468.
(14) (a) Kim, Y.; Joyce, H. J.; Gao, O.; Tan, H. H.; Jagadish, C.; Paladugu, M.; Zou, J.; Suvorova, A. A. *Nano Lett.* **2006**, *6*, 599. (b) Su, J.; Gherasimova, M.; Cui, G.; Tsukamoto, H.; Han, J.; Onuma, T.; Kurimoto, M.; Chichibu, S. F.; Broadbridge, C.; He, Y.; Nurmikko, A. V. *Appl. Phys. Lett.* **2005**, *87*, 183108. (c) Wu, Z. H.; Sun, M.; Mei, X. Y.; Ruda, H. E. *Appl. Phys. Lett.* **2004**, *85*, 657.
(15) Wagner, R. S.; Ellis, W. C. *Appl. Phys. Lett.* **1964**, *4*, 89.
(16) Dubrovskii, V. G.; Cirlin, G. E.; Soshnikov, I. P.; Tonkikh, A. A.; Sibirev, N. V.; Samsonenko, Y. B.; Ustinov, V. M. *Phys. Rev. B* **2005**, *71*, 205325.

(17) Borgström, M. T.; Immink, G.; Ketelaars, B.; Algra, R.; Bakkers, E. *Nat. Nanotechnol.* **2007**, *2*, 541.
(18) Givargizov, E. I. *J. Cryst. Growth* **1975**, *31*, 20.
(19) Dubrovskii, V. G.; Sibirev, N. V.; Suris, R. A.; Cirlin, G. E.; Ustinov, V. M.; Tchernysheva, M.; Harmand, J. C. *Semiconductors* **2006**, *40*, 1075.
(20) Seifert, W.; Borgstrom, M.; Deppert, K.; Dick, K. A.; Johansson, J.; Larsson, M. W.; Martensson, T.; Skold, N.; Svensson, C. P. T.; Wacaser, B. A.; Wallenberg, L. R.; Samuelson, L. *J. Cryst. Growth* **2004**, *272*, 211.
(21) Tambe, M.; Gradečak, S., unpublished.
(22) Three-fold symmetry of the shell, as seen in Figure 3a, suggests that the development of a nonequilateral shell on the equilateral core is likely caused by different growth rates on facets of opposite polarity, but further investigation is needed to confirm this assumption.
(23) Paiano, P.; Prete, P.; Lovergine, N.; Mancini, A. M. *J. Appl. Phys.* **2006**, *100*, 094305.
(24) Chen, C.; Shehata, S.; Fradin, C.; LaPierre, R.; Couteau, C.; Weihs, G. *Nano Lett.* **2007**, *7*, 2584.
(25) Liu, Y.; Shimomura, S.; Sano, N.; Gamo, K.; Adachi, A.; Hiyamizu, S. *Semicond. Sci. Technol.* **1993**, *8*, 2197.
(26) Gottschalch, V.; Leibiger, G.; Benndorf, G.; Herrnberger, H.; Spemann, D. *J. Cryst. Growth* **2004**, *272*, 642.
(27) van Deelen, J.; Bauhuis, G. J.; Schermer, J. J.; Larsen, P. K. *J. Cryst. Growth* **2005**, *284*, 28.
(28) Nomura, Y.; Morishita, Y.; Goto, S.; Katayama, Y.; Isu, T. *Appl. Phys. Lett.* **1994**, *64*, 1123.
(29) Reep, D. H.; Ghandhi, S. K. *J. Electrochem. Soc.* **1983**, *130*, 675.
(30) Hayakawa, T.; Morishima, M.; Chen, S. *Appl. Phys. Lett.* **1991**, *59*, 3321.
(31) Bylander, D. M.; Kleinman, L. *Phys. Rev. B* **1986**, *34*, 5280.

NL080129N